

Review

Near-Infrared Light Driven ZnIn₂S₄-Based Photocatalysts for Environmental and Energy Applications: Progress and Perspectives

Yi Cai ¹, Fangxin Luo ¹, Yujun Guo ¹, Feng Guo ², Weilong Shi ^{3,*} and Shengtao Yang ^{1,*} 

¹ Key Laboratory of Pollution Control Chemistry and Environmental Functional Materials for Qinghai-Tibet Plateau of the National Ethnic Affairs Commission, School of Chemistry and Environment, Southwest Minzu University, Chengdu 610041, China

² School of Energy and Power, Jiangsu University of Science and Technology, Zhenjiang 212003, China

³ School of Material Science and Engineering, Jiangsu University of Science and Technology, Zhenjiang 212003, China

* Correspondence: shiwl@just.edu.cn (W.S.); yangst@swun.edu.cn (S.Y.)

Abstract: Zinc indium sulfide (ZnIn₂S₄), as a significant visible-light-responsive photocatalyst, has become a research hotspot to tackle energy demand and environmental issues owing to its excellent properties of high stability, easy fabrication, and remarkable catalytic activity. However, its drawbacks, including low utilization of solar light and fast photoinduced charge carriers, limit its applications. Promoting the response for near-infrared (NIR) light (~52% solar light) of ZnIn₂S₄-based photocatalysts is the primary challenge to overcome. In this review, various modulation strategies of ZnIn₂S₄ have been described, which include hybrid with narrow optical gap materials, bandgap engineering, up-conversion materials, and surface plasmon materials for enhanced NIR photocatalytic performance in the applications of hydrogen evolution, pollutants purification, and CO₂ reduction. In addition, the synthesis methods and mechanisms of NIR light-driven ZnIn₂S₄-based photocatalysts are summarized. Finally, this review presents perspectives for future development of efficient NIR photon conversion of ZnIn₂S₄-based photocatalysts.

Keywords: ZnIn₂S₄; photocatalysis; hydrogen evolution; near-infrared light



Citation: Cai, Y.; Luo, F.; Guo, Y.; Guo, F.; Shi, W.; Yang, S. Near-Infrared Light Driven ZnIn₂S₄-Based Photocatalysts for Environmental and Energy Applications: Progress and Perspectives. *Molecules* **2023**, *28*, 2142. <https://doi.org/10.3390/molecules28052142>

Academic Editors: Pawan Kumar and Devika Laishram

Received: 15 January 2023

Revised: 17 February 2023

Accepted: 21 February 2023

Published: 24 February 2023



Copyright: © 2023 by the authors. Licensee MDPI, Basel, Switzerland. This article is an open access article distributed under the terms and conditions of the Creative Commons Attribution (CC BY) license (<https://creativecommons.org/licenses/by/4.0/>).

1. Introduction

Photocatalytic technology is recognized as a potential eco-friendly approach to address the issues of environmental pollution and energy shortage by utilizing solar light. A host of photocatalysts have been synthesized for efficient photocatalytic activity, e.g., TiO₂ [1,2], metal oxides [3], metal nitrides/sulfides [4–7], graphitic carbon nitride (g-C₃N₄) [8–10], metal–organic frameworks (MOF) [11,12], and covalent organic frameworks (COF) [13,14]. Recently, zinc indium sulfide (ZnIn₂S₄), as a member of the ternary AB₂X₄ family, aroused researchers' interest in the photocatalysis field [15,16]. It exhibits excellent properties of visible light absorption owing to its suitable band gap (~2.5 eV), which leads to abundant generation of photoinduced carriers under visible light irradiation [17–19]. Additionally, it shows remarkable chemical stability, sharing similar characteristics with other metal sulfides [20,21]. Moreover, it has the properties of stable and easy fabrication, which makes it feasible for practical applications. Benefitting from these advantages, the applications of ZnIn₂S₄ have been reported for water splitting [22–31], CO₂ reduction [32,33], Cr(VI) reduction [34–36], nitrogen reduction, [37–39] pollutant removal [40–43], etc.

Although ZnIn₂S₄ exhibits excellent photocatalytic activity in the UV–visible light range, it has poor photocatalytic activity in near-infrared light (NIR) [44,45] due to its low response towards NIR. The solar spectrum consists of ultraviolet (UV, 300–400 nm), visible (400–700 nm), and near-infrared (NIR, 700–2500 nm) regions, which account for of 5%,

43%, and 52%, respectively [44–46]. Therefore, the NIR light absorption of ZnIn₂S₄-based should be extended to improve solar light utilization, and the fabrication of NIR-responsive ZnIn₂S₄ photocatalysts is the crucial approach to promote its photocatalytic efficiency for further practical applications. There are three mechanisms to promote utilization of near-infrared light by ZnIn₂S₄: (i) constructing narrow bandgap semiconductors such as Ag₂S [47], Ag₂O [48], and Bi₂WO₆ [49], etc. to absorb NIR light directly to generate electron hole carriers for photocatalytic redox reactions; (ii) coupling with up-conversion materials such as carbon quantum dots (CQDs), Cu₂(OH)PO₄, etc., to convert NIR light to high-energy UV–visible light, thus promoting the NIR photocatalytic activity; and (iii) the photothermal effect, in which photothermal composites convert NIR light to thermal energy and boost photocatalytic activity [27,33,50–52]. In order to extend the NIR light absorption range and separate photoinduced charge carriers, several strategies have been applied to fabricate ZnIn₂S₄-based NIR light-driven photocatalysts, including bandgap engineering, construction of narrow optical gap materials, up-conversion, and plasmonic materials [53–56].

Herein, recent progress in NIR-driven ZnIn₂S₄ photocatalysts for the application of hydrogen evolution, pollutant removal, and CO₂ reduction is overviewed. Firstly, different construction strategies of ZnIn₂S₄-based photocatalysts to allow full utilization of NIR in the solar spectrum are comprehensively summarized, including hybrid with narrow optical gap materials, bandgap engineering, up-conversion materials, and plasmonic materials. Focus then turns to the applications of photocatalytic water splitting, organic pollutants removal and CO₂ reduction. Recent research into strategies and applications of NIR-driven ZnIn₂S₄-based photocatalysis is summarized in the table below (Table 1). In addition, this review discusses the mechanisms of ZnIn₂S₄-based NIR light-driven photocatalysts in the respective photocatalytic systems. Finally, current challenges and perspectives for the future development of efficient NIR-responsive ZnIn₂S₄-based photocatalysts are put forward.

Table 1. Summary of NIR-driven ZnIn₂S₄-based NIR photocatalysts for various applications.

Photocatalysts	Broadband Light Harvester	NIR Photon Capture Method	Light Source	Extended Wavelength	Application	Ref.
ZIS/AgIn ₅ S ₈	AgIn ₅ S ₈	Hybrid with NOGMs	500 W tungsten halogen lamp	>420 nm	Dye degradation	[57]
ZIS/CuInS ₂	CuInS ₂	Hybrid with NOGMs	300 W Xe-lamp	>420 nm	H ₂ production	[53]
Zn-defective ZIS-Laponite	Laponite	BGE	Visible light	400–800 nm	Dye degradation	[54]
NaYF ₄ :Yb,Tm/ZIS	NaYF ₄ :Yb,Tm	Up-conversion effect	300 W Xe-lamp	≥800 nm	CO ₂ reduction	[58]
NaYF ₄ :Yb ³⁺ /Tm ³⁺ @ZIS	NaYF ₄ :Yb ³⁺ /Tm ³⁺	Up-conversion effect	300 W Xe-lamp	<400 nm 400–800 nm >800 nm	H ₂ production	[55]
CQDs/ZIS	CQDs	Up-conversion effect	150 W infrared lamp	N.A.	Tetracycline hydrochloride degradation	[59]
CQDs ZIS/BiOCl	CQDs	Up-conversion effect	300 W Xe-lamp 150 W infrared lamp	>420 nm <700 nm	Antibiotics removal	[60]
WO _{3-x} /ZIS	WO _{3-x}	SPR	300 W Xe lamp	400–1100 nm	H ₂ production	[56]
K ₃ PW ₁₂ O ₄₀ @ZIS/Ag ₂ S	Ag ₂ S	SPR	300 W Xe-lamp	>420 nm	H ₂ production Tetracycline hydrochloride degradation	[61]
W ⁵⁺ –W ⁵⁺ pair induced of W ₁₈ O ₄₉ /ZIS	W ₁₈ O ₄₉	SPR	Simulated solar light NIR light	>420 nm >700 nm	H ₂ production	[62]
Au@Pt/ZIS	Au@Pt	SPR	300 W Xe-lamp	≥420 nm	H ₂ production	[63]
ZIS/N-doped graphene	N-doped graphene	Photothermal effect	300 W Xe-lamp	>420 nm	CO ₂ capture CO ₂ photoreduction	[33]
SnSe/ZIS	SnSe	Photothermal effect	300 W Xe lamp	400–1100 nm	H ₂ production	[50]

ZIS: ZnIn₂S₄; NOGMs: narrow optical gap materials; BGE: bandgap engineering; SPR: surface plasmon resonance; CQDs: carbon quantum dots.

2. Hybrid with Narrow Optical Gap Materials

Narrow optical gap materials (NOGMs, e.g., Ag_2O , CuInS_2 and black phosphorus) have an inherent response to visible–NIR light. However, the rapid recombination of photo-induced carriers and band positions limits their application in photocatalysis. Therefore, the use of traditional narrow bandgap semiconductors by itself is inefficient and impractical for photocatalytic utilization. Constructing binary or ternary heterostructures photocatalysts consequently served as a potential candidate for achieving distinguished photocatalytic performance. In recent years, more attention has focused on coupling ZnIn_2S_4 with NOGMs for NIR light-driven photocatalysis as a result of enhanced NIR-driven photoactivity and photo-generated charge carriers.

Metal chalcogenides exhibit a broad-band absorption property in the visible to NIR range with a narrow bandgap. For instance, Xu et al. [57] fabricated $\text{AgIn}_5\text{S}_8/\text{ZnIn}_2\text{S}_4$ heteromicrospheres with visible–NIR absorption characteristics in the range of 200–810 nm synthesized by a partial cation exchange method. TEM (transmission electron microscopy, (Figure 1a)) and HRTEM (high-resolution transmission electron microscopy, (Figure 1b)) show that AgIn_5S_8 flake-like structures were distributed on the surface of ZnIn_2S_4 , proving the formation of a heterojunction. The absorption edge of heterostructure shows the redshift from 593 nm to 810 nm compared to pristine ZnIn_2S_4 , and the Rhodamine B (RhB) photodegradation rate reached 99.2% within 50 min. Additionally, the thickness of AgIn_5S_8 could be a crucial factor affecting the photodegradation efficiency from the joint results of photodegradation and X-ray photoelectron spectroscopy (XPS) analysis [57]. In another study, Yu et al. [53] prepared $\text{ZnIn}_2\text{S}_4@\text{CuInS}_2$ microflowers through a two-step hydrothermal approach, and HRTEM images (Figure 1c,d) displayed that CuInS_2 wrapped on the surface of ZnIn_2S_4 , which indicated the successful integration between CuInS_2 and ZnIn_2S_4 . The absorption region was extended from visible light to the NIR region owing to the good construction of CuInS_2 and ZnIn_2S_4 . Moreover, further characteristics such as the photocurrent and chemical impedance spectroscopy, etc., led to the generation of more photoinduced electrons and a higher performance of charge transfer. Consequently, the ZnIn_2S_4 integrated with 0.05% CuInS_2 exhibited a remarkable hydrogen evolution rate of $1168 \mu\text{mol g}^{-1}$ under $\lambda > 420 \text{ nm}$ light irradiation. The mechanism (Figure 1e) demonstrated that the remarkable photocatalytic activity was contributed to by the built-in electric field between ZnIn_2S_4 and CuInS_2 , which created a larger interface contact area and thus promoted charge separation and transfer. Moreover, a slight decrease in hydrogen evolution photoactivity was observed in the recycling reactions due to the photocorrosion effect of the hole consumption [64,65] and stability of the $\text{ZnIn}_2\text{S}_4@\text{CuInS}_2$ materials was confirmed by SEM and TEM carried out before and after the reactions.

Research on hybrid with narrow optical gap materials is in its early stages, and combined strategies should be considered to balance the benefits of broad solar light absorption by NOGMs due to its narrow bandgap, and its drawbacks of fast photoinduced carrier recombination. Moreover, the innovative design of ZnIn_2S_4 -based photocatalysts could avoid their photocorrosion and promote their recycling and stability performance.

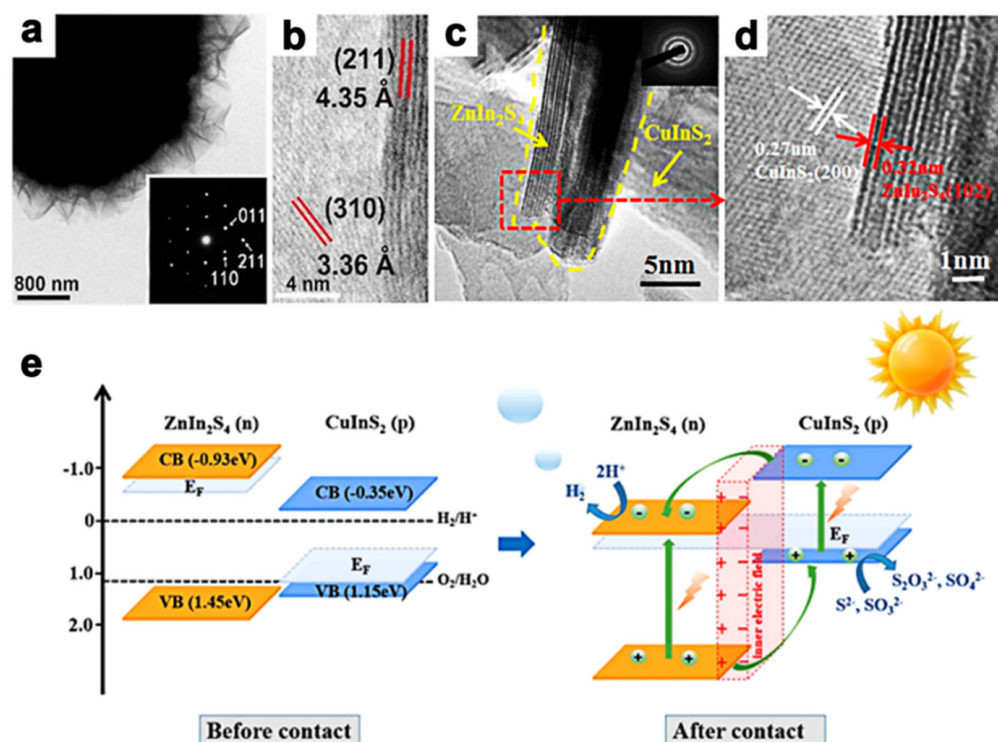


Figure 1. TEM (a) and HRTEM (b) of AgIn₅S₈/ZnIn₂S₄ heteromicrospheres. Reprinted with permission from Ref. [57]. Copyright 2015, Royal Society of Chemistry. (c,d) HRTEM of ZnIn₂S₄@CuInS₂ composites [53]. (e) Schematic diagrams of the formation of *p*–*n* junction and proposed charge separation process in the ZnIn₂S₄@CuInS₂ core–shell photocatalysts. Reprinted with permission from Ref. [53]. Copyright 2020, American Chemical Society.

3. Bandgap Engineering

In addition to incorporating NIR-spectrum response semiconductors, bandgap engineering (BGE) is a promising strategy for fabricating NIR-responsive ZnIn₂S₄. The introduction of atom doping, defects, and disorders is a common approach applied to modify the ZnIn₂S₄ electronic structure and composition stoichiometry and thus enhance the light utilization to the NIR range. However, only a few cases of bandgap engineering of ZnIn₂S₄ have been reported for construction of NIR-responsive photocatalysts. For instance, Hill et al. reported the formation of Zn-defective ZnIn₂S₄–Laponite heterostructures due to Mg²⁺ leached from Laponite in the synthesis process (Figure 2a); leached Mg²⁺ replaced the Zn in ZnIn₂S₄ owing to their similar ionic radii, which led to the formation of Zn defects in ZnIn₂S₄. Due to this engineering defect, the absorption range of the ZnIn₂S₄–Laponite samples was broadened from UV to NIR at approximately 800 nm (Figure 2b). Furthermore, higher charge separation efficiency and greater photoinduced charge were observed by using transient photocurrent measurements and electrochemical impedance spectroscopy (EIS) methods. Eventually, the photocatalytic degradation of methyl orange (MO) by ZnIn₂S₄–Laponite was 3.3 times more efficient than pure ZnIn₂S₄, which could be attributed to the formation of Zn vacancies in ZnIn₂S₄ acting as electron capture centers and therefore promoting the photoinduced charge separation [54].

To date, beyond introducing defects, other bandgap engineering methods such as atom doping and disorders, etc., on ZIS have not yet been explored. These bandgap engineering approaches could be feasible ways to enhance the absorption of NIR light and therefore promote photocatalytic efficiency.

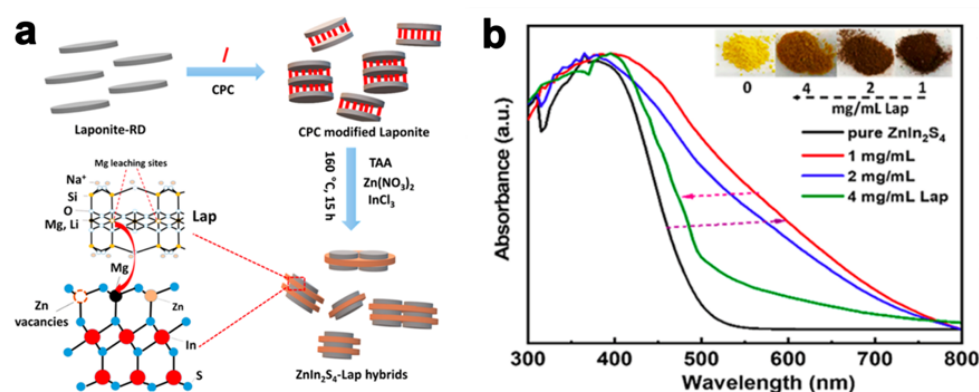


Figure 2. (a) Schematic illustration of ZnIn_2S_4 -Laponite synthesis, where CPC and Lap represent cetylpyridinium chloride and laponite, respectively. (b) UV-vis diffuse reflectance spectra of inset samples with different amounts of Laponite at 1, 2, and 4 mg mL^{-1} , respectively. Reprinted with permission from Ref. [54]. Copyright 2021, American Chemical Society.

4. Up-Conversion Materials

Up-conversion is an anti-Stokes luminescence process that derives from sensitized triplet-triplet annihilation, converting low-energy pump photons to higher-energy emission (UV or visible light photons). The up-conversion process makes it feasible to exploit the solar spectrum owing to the conversion of NIR light to UV or visible light. Therefore, constructing ZnIn_2S_4 -based up-conversion materials is a promising approach to developing NIR-responsive photocatalysts. Among up-conversion materials, lanthanide (Ln) and carbon dots (CDs) are the most attractive to trigger NIR light-driven ZnIn_2S_4 -based photocatalysts.

The up-conversion system utilizes the solar spectrum by the following mechanisms: excited-state absorption (ESA), photon avalanche (PA), energy migration-mediated UC (EMU), and energy transfer up-conversion (ETU) (Figure 3). Specifically, the ETU system includes successive energy transfer (SET), cross-relaxation (CR), and cooperative up-conversion (CU). Lanthanide (Ln)-based UC materials generally include two types of ions as the donor and acceptor, respectively; therefore the ion composition and matrix could be prominent factors for their efficiency. Host matrices such as NaYF_4 , NaGdF_4 , and CaF_2 are commonly used, as well as ion compositions of Yb/Er, Yb/Tm, and Yb/Ho. Moreover, direct Ln ion doping and heterostructure development are common strategies to develop Lanthanide materials with ZnIn_2S_4 . Shi and Guo et al. [55] have successfully prepared a three-dimensional $\text{NaYF}_4:\text{Yb}^{3+}/\text{Tm}^{3+}/\text{ZnIn}_2\text{S}_4$ (NYF@ZIS) material through a facile hydrothermal and water-bathing process, successfully leading to ZnIn_2S_4 coating onto the surface of hexagonal prisms (Figure 4a–f). NYF@ZIS exhibited intensive optical absorption ranging from 650 to 1000 nm, giving the property of utilizing NIR light. The UC process is ascribed to the energy transfer between Yb^{3+} and Tm^{3+} ions, and eventually, ZnIn_2S_4 was excited through the ET process from the up-conversion luminescence agent of $\text{NaYF}_4:\text{Yb}^{3+}/\text{Tm}^{3+}$. Furthermore, the separation of photogenerated charge carriers was promoted by the construction of ZnIn_2S_4 and $\text{NaYF}_4:\text{Yb}^{3+}/\text{Tm}^{3+}$. In this way, the application of H_2 evolution for $\text{NaYF}_4:\text{Yb}^{3+}/\text{Tm}^{3+}/\text{ZnIn}_2\text{S}_4$ was tested under NIR light ($\lambda > 800$ nm) irradiation and showed an evolution rate of $17.81 \mu\text{mol g}^{-1} \text{h}^{-1}$. Coupling up-conversion nanoparticles (UCNPs, $\text{NaYF}_4:\text{Yb}/\text{Tm}$) enhanced the photocatalytic performance of ZnIn_2S_4 according to Li and Idris et al. [58], in which UCNPs absorbed NIR photons and emitted UV-visible photons to excite ZnIn_2S_4 . Ultimately, the photoinduced energy transfer gave rise to remarkable CO and CH_4 production rates of 1500 and $220 \text{ nmol g}^{-1} \text{h}^{-1}$ under NIR-light illumination. Overall, the Ln doping promoted ZnIn_2S_4 photocatalytic performance by not only increasing available high-energy photons with the absorption range through up-conversion luminescence approaches but also by morphology modification for efficient separation and migration of photoinduced charge carriers.

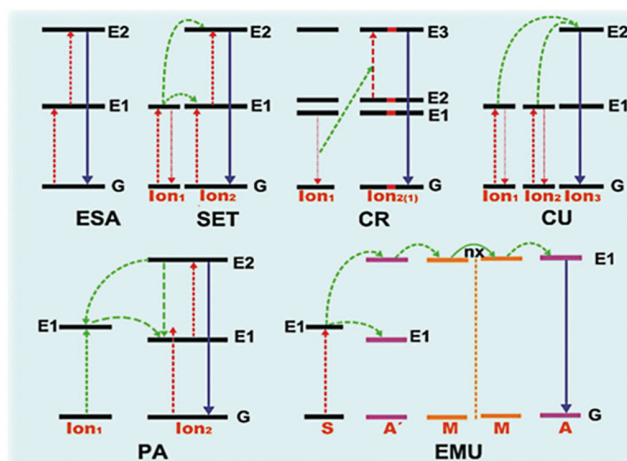


Figure 3. Principal diagram for the up-conversion processes of Ln^{3+} -doped crystals, including excited-state absorption (ESA), successive energy transfer (SET), cross-relaxation (CR), cooperative up-conversion (CU), photon avalanche (PA), energy migration-mediated UC (EMU) mechanisms. The red, green, and purple lines stand for photon excitation, energy transfer, and emission processes, respectively. Reprinted with permission from Ref. [66]. Copyright 2021, John Wiley and Sons.

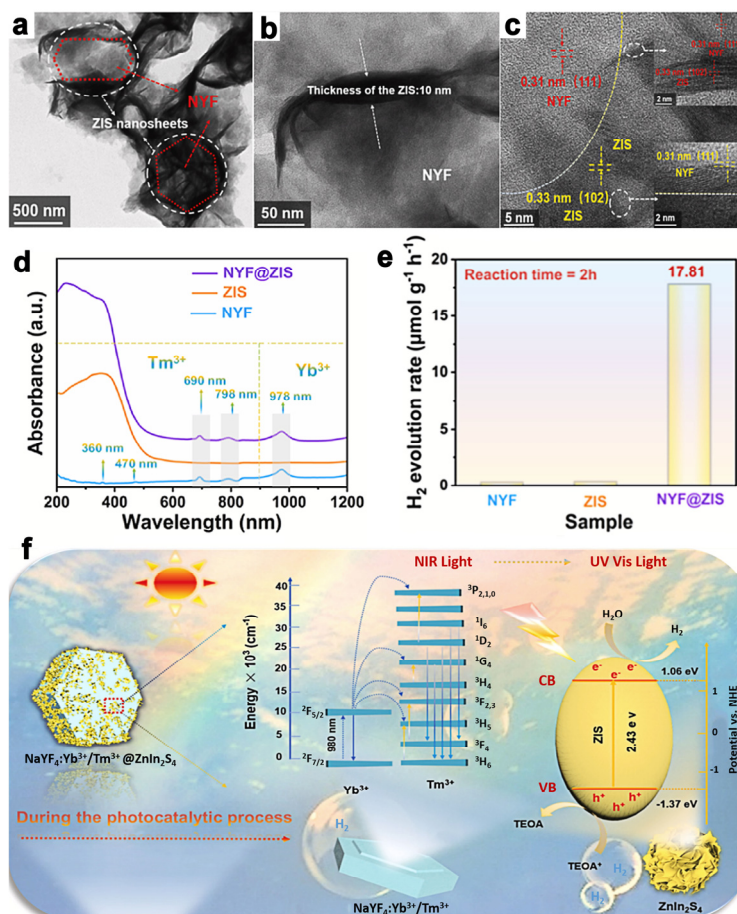


Figure 4. (a,b) TEM and (c) HRTEM images of NYF@ZnIn₂S₄ composite. (d) UV-vis-NIR absorption spectra of ZnIn₂S₄, NYF and NYF@ZnIn₂S₄ composite. (e) Time-dependent photocatalytic hydrogen production curves and hydrogen evolution rates of ZnIn₂S₄, NYF, and NYF@ZnIn₂S₄ composite under NIR ($\lambda > 800$ nm) light irradiation. (f) Mechanism of photocatalytic H₂ evolution for NYF@ZnIn₂S₄ materials under NIR light illumination. Reprinted with permission from Ref. [55]. Copyright 2022, Elsevier.

Besides Ln-based ZnIn_2S_4 construction, carbon dots (CDs) are another up-conversion material for efficient sunlight utilization, which possesses properties of low toxicity, up- and down-conversion fluorescent, good electron transfer, and excellent photostability [67–70]. Xu et al. [59] constructed carbon quantum dots doped ZnIn_2S_4 nanoflowers (ZIS/CQDs) with a wide light response range through a simple in situ hydrothermal synthesis approach (Figure 5a). It demonstrated remarkably expanded absorption attributed to its up-converted mechanism, and the suppression of photoexcited charge recombination owing to the CQDs' performance of photon harvest and transportation. Additionally, the doping content of CQDs also affected the photocatalytic removal efficiency of tetracycline hydrochloride (TCH), and the highest degradation rate reached almost three times higher than pure ZnIn_2S_4 irradiated under NIR light.

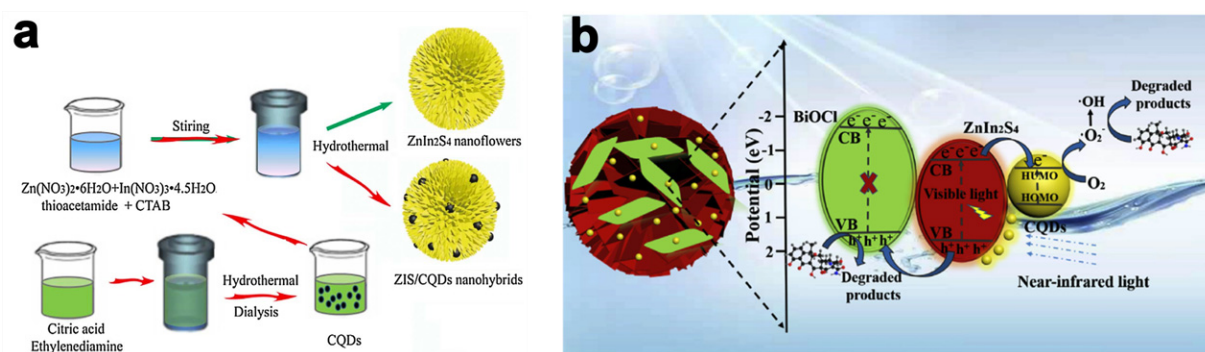


Figure 5. (a) Schematic illustration for the preparation method of $\text{ZnIn}_2\text{S}_4/\text{CQDs}$ composites. Reprinted with permission from Ref. [59]. Copyright 2018, Elsevier. (b) Photocatalytic reaction mechanism of $\text{CQDs}/\text{ZnIn}_2\text{S}_4/\text{BiOCl}$ heterostructures for antibiotic removal at visible and NIR region. Reprinted with permission from Ref. [60]. Copyright 2019, Elsevier.

CQDs promoted the photocatalytic degradation performance of $\text{CQDs}/\text{ZnIn}_2\text{S}_4/\text{BiOCl}$ for antibiotic removal at visible and NIR regions, as reported by Lu et al. [60], in which CQDs modified 2D BiOCl nanosheets/2D layered flower-like ZnIn_2S_4 with van der Waals (VDW) force in between. The as-prepared $\text{CQDs}/\text{ZnIn}_2\text{S}_4/\text{BiOCl}$ heterostructures exhibited noteworthy degradation rates that were 42.5, 2.75, and 1.94 more times efficient than those of pristine BiOCl , ZnIn_2S_4 , and $\text{ZnIn}_2\text{S}_4/\text{BiOCl}$ photocatalysts, respectively. For the reaction mechanisms in $\text{CQDs}/\text{ZnIn}_2\text{S}_4/\text{BiOCl}$, CQDs absorbed NIR photons and emitted visible light photons to excite ZnIn_2S_4 , resulting in electron migration from the valence band to the conduction band. On the one hand, the electrons migrated to CQDs reacting with oxygen in the water to produce reactive $\cdot\text{O}_2^-$ and finally reacted with antibiotic compounds. On the other hand, holes in VB of ZnIn_2S_4 transferred to BiOCl and degraded pollutants (Figure 5b). The enhanced photocatalytic performance was attributed to the van der Waals forces between ZnIn_2S_4 and BiOCl , as well as the introduction of CQDs, which acted as electron acceptors, extended the light absorption edge to NIR and finally boosted photoinduced charge migration due to its up-conversion luminescence ability. Additionally, several approaches including electron spin-resonance spectroscopy (ESR), active species trapping experiments, and high-performance liquid chromatography–tandem mass spectrometry (LC–MS/MS), were carried out to elucidate the photocatalytic degradation pathway of antibiotics (TC, CIP, and OTC) and revealed that the reactive species ($\cdot\text{O}_2^-$, $\cdot\text{OH}$, and holes) played important roles in the degradation processes.

In general, although the up-conversion strategy is a promising way to promote ZnIn_2S_4 photocatalytic efficiency, it requires further modification for practical application. Based on the mechanism of up-conversion, improving the light overlap of Ln-based materials or carbon quantum dots emitted and ZnIn_2S_4 absorbed promotes the enhancement of solar energy utilization. Therefore, up-conversion materials with wide light absorption and photostability are needed for higher photocatalytic efficiency.

5. Surface Plasmon Resonance

Surface plasmon resonances (SPR) or localized surface plasmon resonances (LSPR) is defined as the electron coherent oscillations in metal nanoparticles in response to visible–NIR light irradiation (Figure 6a) [71,72]. On the one hand, the SPR effect triggered by plasmonic metals promotes the photocatalytic ability by absorbing a broader light range, and therefore, the process is affected by the size, shape, and dielectric environment of nanoparticles. Both light scattering and light concentration are essential to the absorption edge extension of photocatalysts by increasing the optical path owing to light trapping or photonic effects (Figure 6b) [72]. On the other hand, direct electron injection energy transfer (DET) and plasmon-induced energy transfer (PIRET) systems are constructed by integrating nanoparticles with semiconductors' heterostructure to extend the light-response region, as well as accelerating charge carrier transfer in between (Figure 6b) [71,73]. Noble nanoparticles, such as Au, Ag, and Pt, are commonly introduced to form heterostructures resulting in the enhancement of ZnIn₂S₄ photocatalytic activity. Yin et al. fabricated assembling core-shell Au@Pt nanoparticles on 3D ZnIn₂S₄ microsphere composites by following multiple steps, first by using citrate reduction and solvothermal methods to form Au nanoparticles and ZnIn₂S₄, respectively, and obtain Au@Pt nanoparticles via electrostatic interaction force and eventually collect composites attributed to the electrostatic force and assist the precursors (Figure 6c) [63]. As shown in Figure 6c, the absorption edge of Au@Pt/ZnIn₂S₄ has been extended from the visible to the NIR light region compared with pure ZnIn₂S₄ and Au@Pt since the Au@Pt serves as the secondary light source by concentrating photons to ZnIn₂S₄, thus generating an EM field with higher energy than therefore the process is affected by the size, shape, and dielectric environment of nanoparticles surrounding light [74–76], which further promotes the utilization of light spectrum. Moreover, the electron hole separation efficiency is accelerated because electrons from both ZnIn₂S₄ and Au transfer to Pt nanoparticles according to the energy-band scheme (Figure 6d,e). Benefiting from these mechanisms above, Au@Pt/ZnIn₂S₄ experiences 10 times greater hydrogen evolution efficiency compared with pure ZnIn₂S₄ under vis–NIR light irradiation.

In addition to noble nanoparticles, nonmetallic semiconductors show a plasmonic effect owing to the properties of element doping or lattice vacancies such as Cu_{2-x}S, MoO_{3-x}, WO_{3-x}, and W₁₈O₄₉ [77–81]. Among them, W₁₈O₄₉ has strong absorption in the visible–NIR wavelengths (Figure 7a) and thus is a promising candidate for developing ZnIn₂S₄ NIR hybrid photocatalysts as a result of sufficient vacancy on its surface [62]. For example, Zhang et al. [62] prepared the W₁₈O₄₉/ZnIn₂S₄ composites (Figure 7b,c) with a full-spectrum sunlight response with excellent hydrogen evolution under UV and NIR light illumination (Figure 7d). The mechanisms of W₁₈O₄₉/ZnIn₂S₄ for hydrogen evolution were proposed as shown in Figure 7e,f. The DFT calculation is conducted to prove that W⁵⁺-W⁵⁺ pairs are the prerequisite for the LSPR effect of W₁₈O₄₉. Multiple additional approaches, such as ultrafast transient absorption spectroscopy (TA) and ESR, are applied to investigate the mechanisms, and the results show that W₁₈O₄₉ captures two photons to excite ZnIn₂S₄, which provides more opportunity for ZnIn₂S₄ to utilize solar spectrum. Moreover, as in the ultrafast transient absorption spectroscopy (TA) measurement, in the plots of pure ZnIn₂S₄ (Figure 7g) and W₁₈O₄₉/ZnIn₂S₄ (Figure 7h) with the pump light at 400 nm, the ZnIn₂S₄ image exhibits a higher concentration of short-lived electrons than that of W₁₈O₄₉/ZnIn₂S₄ at the signal range from 550 to 750 nm, which indicates that more photoinduced electrons recombine with holes in the ZnIn₂S₄ than W₁₈O₄₉/ZnIn₂S₄. In this way, it is concluded that in the W₁₈O₄₉/ZnIn₂S₄ heterostructure, the recombination of electrons and holes in ZnIn₂S₄ is suppressed, and thus, the transfer efficiency of photoexcited charge carriers is accelerated due to the Z-scheme construction of W₁₈O₄₉ and ZnIn₂S₄.

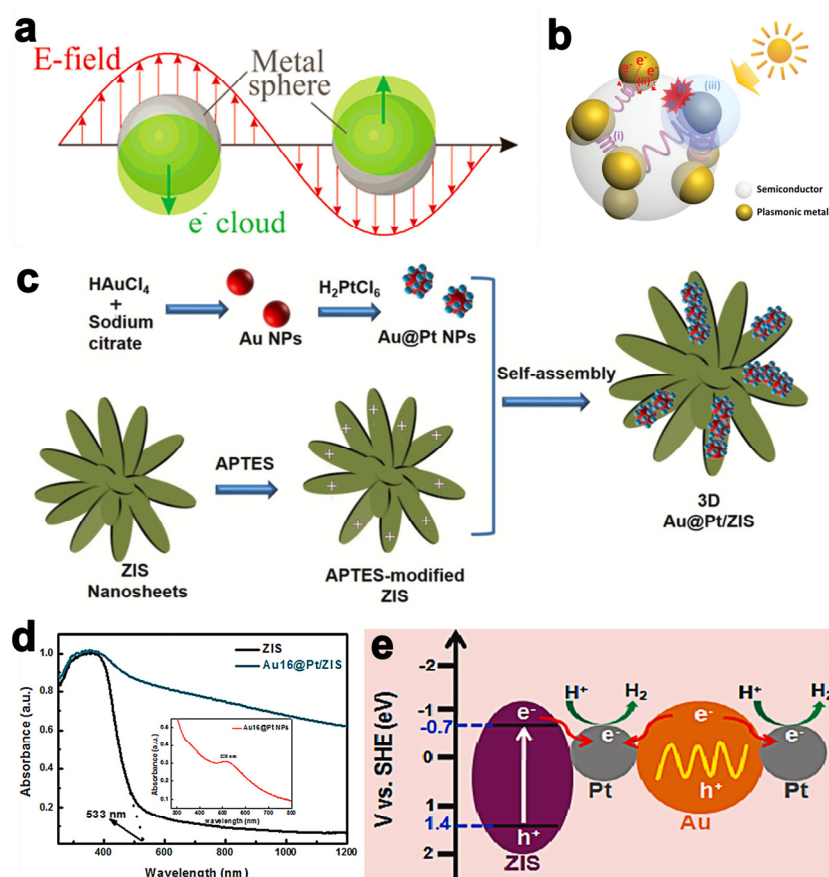


Figure 6. (a) Schematic illustration of plasmon oscillation on a plasmonic metal sphere [71]. (b) Mechanisms for photonic promotion in plasmonic nanoparticles–semiconductor heterostructures, including light scattering and concentration (i), direct electron injection energy transfer (DET) (ii), and plasmon-induced energy transfer (PIRET) (iii). Reprinted with permission from Ref. [71]. Copyright 2015, John Wiley and Sons. (c) Schematic illustration of the Au@Pt/ZnIn₂S₄ composites preparation. (d) UV–vis–NIR spectra of ZnIn₂S₄ and Au@Pt/ZnIn₂S₄. Inset is the absorption spectrum of colloidal Au@Pt nanoparticles. (e) Proposed excitation scheme for the hydrogen production of Au@Pt/ZnIn₂S₄ composites. Reprinted with permission from Ref. [63]. Copyright 2021, Elsevier.

Apart from W₁₈O₄₉, WO_{3-x} with lattice vacancy also has a surface plasmon resonance (SPR) effect owing to its collective oscillations of free carriers. Ni et al. [56] fabricated WO_{3-x}/ZnIn₂S₄ heterojunctions via a straightforward scaled-up process for H₂ production photoactivity. The interaction of WO_{3-x} with ZnIn₂S₄ is beneficial for expanding the absorption light from UV–visible to NIR light range, which gives the photocatalysts capability to generate H₂ by splitting water throughout the full solar spectrum. WO_{3-x}/ZnIn₂S₄ photocatalysts exhibit a remarkable H₂ production rate of 20,957 μmol h⁻¹ g⁻¹, which is 2.7 times higher than that of pure ZnIn₂S₄ under simulated sunlight illumination. Together with the results of the EIS (Figure 8a) and PL measurements (Figure 8b), the WO_{3-x}/ZnIn₂S₄—with a smaller resistance curve and weaker PL emission than pure ZnIn₂S₄—indicates more efficient electron transfer and charge separation. Additionally, the proposed mechanism (Figure 8c) reveals that after absorbing UV–vis–NIR light, electrons in the VB of WO_{3-x} and ZnIn₂S₄ migrate to their respective CB, then electrons and holes in the VB of ZnIn₂S₄ combine together as a result of the electron transfer from CB of WO_{3-x}. The H₂ production eventually occurs in the CB of ZnIn₂S₄. The ΔG_{H⁺} value of the WO_{3-x}/ZnIn₂S₄ hybrid calculated by the DFT method further confirms the mechanism (Figure 8d).

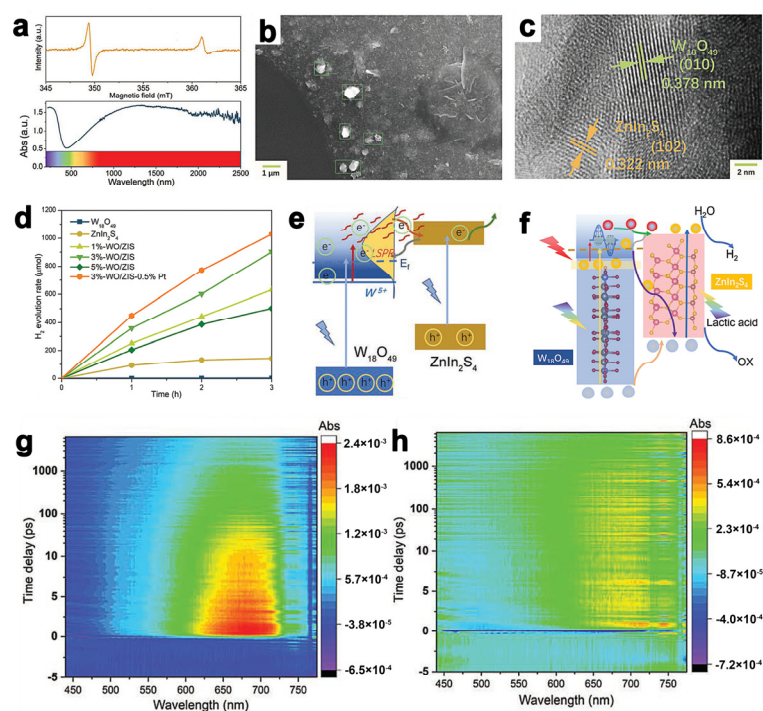


Figure 7. (a) Absorption spectra of $W_{18}O_{49}$. (b) SEM and (c) HRTEM images of $W_{18}O_{49}/ZnIn_2S_4$. (d) Time-dependent photocatalytic H_2 evolution curves of different samples under simulated sunlight irradiation. (e) Schematic diagram of electron transition of $W_{18}O_{49}/ZnIn_2S_4$ under 400 nm irradiation. (f) The schematic diagram for photocatalytic H_2 evolution by $W_{18}O_{49}/ZnIn_2S_4$ heterojunction. Pseudocolor TA plots of (g) $ZnIn_2S_4$ and (h) $W_{18}O_{49}/ZnIn_2S_4$ under 400 nm irradiation. Reprinted with permission from Ref. [62]. Copyright 2022, John Wiley and Sons.

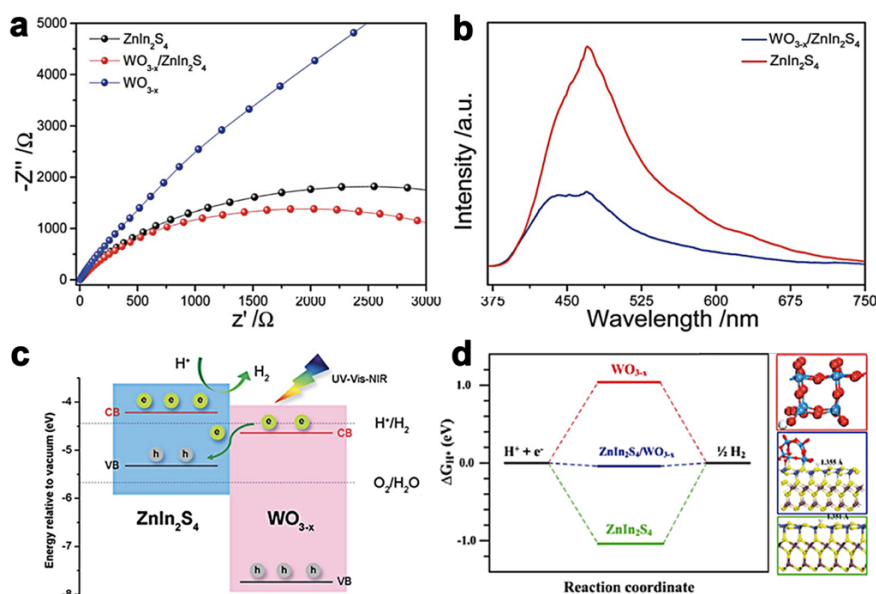


Figure 8. (a) Electrochemical impedance spectroscopy (EIS). (b) Photoluminescence and (c) diagram of the proposed H_2 production mechanism for $WO_{3-x}/ZnIn_2S_4$. (d) DFT calculation ΔG_{H^+} values and adsorption property of $ZnIn_2S_4$, WO_{3-x} and $WO_{3-x}/ZnIn_2S_4$. Reprinted with permission from Ref. [56]. Copyright 2021, Royal Society of Chemistry.

In another study, Zhou et al. [61] synthesized a novel photocatalyst of $K_3PW_{12}O_{40}@ZnIn_2S_4$ and further loaded Ag_2S quantum dots via the hydrothermal method followed by a cation exchange process, construction a dodecahedral $K_3PW_{12}O_{40}$ capped with flower-like

ZnIn₂S₄, and finally by distribution of Ag₂S dots on the surface (Figure 9a). The introduction of Ag₂S quantum dots led to a red shift from visible light to NIR light with higher optical absorption intensity (Figure 9b) compared with pristine ZnIn₂S₄ and K₃PW₁₂O₄₀, respectively. It displayed high photocatalytic performance and photostability both for tetracycline hydrochloride and H₂ production activity, notably with an optimal photodegradation rate of 99% (Figure 9c) and hydrogen production rate of 2.1 mmol g⁻¹ h⁻¹. Overall, the boosted NIR photoactivity was attributed to the SPR effect of Ag₂S quantum dots (Figure 9d), which have extensive absorption of NIR light. Furthermore, the unique structure of K₃PW₁₂O₄₀@ZnIn₂S₄/Ag₂S provided more efficient light scattering and reactive reaction sites and prolonged the lifetime of photoinduced charge carriers.

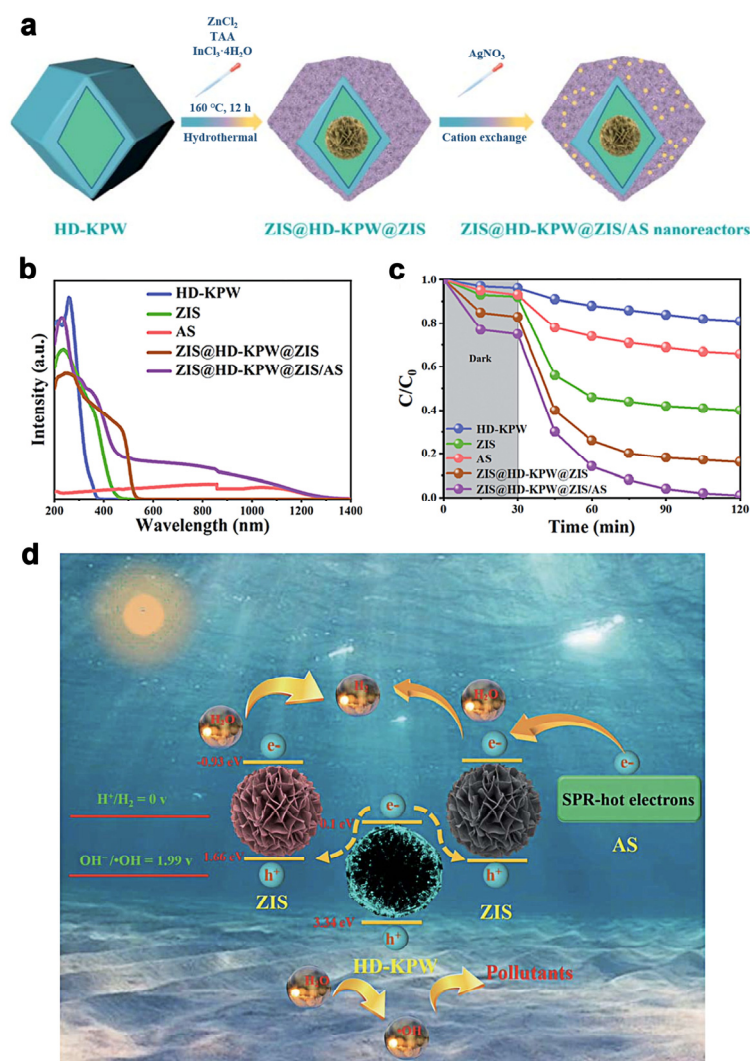


Figure 9. (a) Schematic illustration of K₃PW₁₂O₄₀@ZnIn₂S₄/Ag₂S preparation, hollow dodecahedral K₃PW₁₂O₄₀, ZnIn₂S₄ and Ag₂S were named HD-KPW, ZIS and AS. (b) UV-Vis-NIR diffuse reflectance spectra and (c) tetracycline hydrochloride photodegradation of K₃PW₁₂O₄₀, ZnIn₂S₄, Ag₂S, K₃PW₁₂O₄₀@ZnIn₂S₄, and K₃PW₁₂O₄₀@ZnIn₂S₄/Ag₂S, respectively. (d) Proposed mechanism of K₃PW₁₂O₄₀@ZnIn₂S₄/Ag₂S heterojunctions for pollutant removal and hydrogen production. Reprinted with permission from Ref. [61]. Copyright 2022, Royal Society of Chemistry.

6. Conclusions and Prospects

In recent years, ZnIn₂S₄ has come to be regarded as a promising photocatalyst due to its excellent properties of low cost, facile synthesis, and environmental harmlessness. Benefiting from these features, it has been widely applied in organic pollutant removal, hydrogen evolution, CO₂ reduction, etc. Nevertheless, its photocatalytic efficiency is far from

satisfactory due to its limited NIR light absorption, and thus, the fabrication of ZnIn₂S₄-based NIR photocatalysts is highly desired to enhance NIR light utilization. The present review summarizes strategies for promoting the extension of ZnIn₂S₄ response into the NIR range, as well as an overview of their fabrication methods, mechanisms for reactions, and applications. Strategies including hybrid with narrow optical gap materials, bandgap engineering, up-conversion materials, and surface plasmon resonance are overviewed to extend ZnIn₂S₄'s NIR light absorption and boost its solar energy efficiency. In addition, the photocatalytic applications of NIR-driven ZnIn₂S₄-based photocatalysts have been reported in the field of hydrogen production, pollutant removal, and CO₂ reduction.

Despite the promising results that have been accomplished, there remain several primary challenges to overcome. (1) The NIR absorption range of ZnIn₂S₄-based photocatalytic systems should be further expanded to make better utilization of solar energy. More research on constructing ZnIn₂S₄ with up-conversion or SPR materials is needed to enhance the absorption range. (2) Photosensitizers can absorb NIR photons to generate electrons, and if combined with ZnIn₂S₄-based photocatalysts, could further promote the NIR utilization of the ZnIn₂S₄-hybrid photosystems. However, no fabrications and applications of photosensitizers/ZnIn₂S₄ composites have yet been reported. More efforts could be devoted to this photocatalysis direction. (3) The light absorption intensity of the NIR ZnIn₂S₄-based photocatalysts is relatively inadequate, which results in low efficiency from solar to chemical energy. Therefore, modifications to the structure, morphology, and composition of SPR materials should be explored, which could enhance the NIR intensity by concentrating light and extending the absorption edge. (4) The mechanism of ZnIn₂S₄-based photosystems for NIR absorption is unclear; further approaches such as DFT calculations and advanced technics are strongly recommended to investigate the NIR absorption principles. (5) Future lab-scale and practical research on constructing easy-synthesis and environmentally friendly NIR ZnIn₂S₄-based photocatalysts is required with the aim to apply the photocatalysis technology to industrial applications.

Author Contributions: Conceptualization, Y.C., W.S. and S.Y.; resources and visualization, F.L.; Y.G. and F.G.; writing—original draft preparation, Y.C.; writing—review and editing, Y.C. and F.G.; funding acquisition, Y.C., W.S. and S.Y. All authors have read and agreed to the published version of the manuscript.

Funding: This research was funded by Southwest Minzu University Research Startup Funds (RQD2022054) and National Natural Science Foundation of China (No. 22006057).

Conflicts of Interest: The authors declare no conflict of interest.

References

1. Fujishima, A.; Honda, K. Electrochemical Photolysis of Water at a Semiconductor Electrode. *Nature* **1972**, *238*, 37. [[CrossRef](#)] [[PubMed](#)]
2. Dhakshinamoorthy, A.; Navalon, S.; Corma, A.; Garcia, H. Photocatalytic CO₂ Reduction by TiO₂ and Related Titanium Containing Solids. *Energy Environ. Sci.* **2012**, *5*, 9217–9233. [[CrossRef](#)]
3. Hisatomi, T.; Kubota, J.; Domen, K. Recent Advances in Semiconductors for Photocatalytic and Photoelectrochemical Water Splitting. *Chem. Soc. Rev.* **2014**, *43*, 7520–7535. [[CrossRef](#)] [[PubMed](#)]
4. Zhen, C.; Chen, R.; Wang, L.; Liu, G.; Cheng, H.M. Tantalum (Oxy)Nitride Based Photoanodes for Solar-Driven Water Oxidation. *J. Mater. Chem. A* **2016**, *4*, 2783–2800. [[CrossRef](#)]
5. Wang, J.; Lin, S.; Tian, N.; Ma, T.; Zhang, Y.; Huang, H. Nanostructured Metal Sulfides: Classification, Modification Strategy, and Solar-Driven CO₂ Reduction Application. *Adv. Funct. Mater.* **2021**, *31*, 2008008. [[CrossRef](#)]
6. Yang, Y.; Que, W.; Zhang, X.; Yin, X.; Xing, Y.; Que, M.; Zhao, H.; Du, Y. High-Quality Cu₂ZnSnS₄ and Cu₂ZnSnSe₄ Nanocrystals Hybrid with ZnO and NaYF₄: Yb, Tm as Efficient Photocatalytic Sensitizers. *Appl. Catal. B Environ.* **2017**, *200*, 402–411. [[CrossRef](#)]
7. Yang, Y.; Que, W.; Zhang, X.; Xing, Y.; Yin, X.; Du, Y. Facile Synthesis of ZnO/CuInS₂ Nanorod Arrays for Photocatalytic Pollutants Degradation. *J. Hazard. Mater.* **2016**, *317*, 430–439. [[CrossRef](#)]
8. Fu, J.; Yu, J.; Jiang, C.; Cheng, B. G-C₃N₄-Based Heterostructured Photocatalysts. *Adv. Energy Mater.* **2018**, *8*, 1701503. [[CrossRef](#)]
9. Ong, W.J.; Tan, L.L.; Chai, S.P.; Yong, S.T.; Mohamed, A.R. Surface Charge Modification via Protonation of Graphitic Carbon Nitride (g-C₃N₄) for Electrostatic Self-Assembly Construction of 2D/2D Reduced Graphene Oxide (RGO)/g-C₃N₄ Nanostructures toward Enhanced Photocatalytic Reduction of Carbon Dioxide to Methane. *Nano Energy* **2015**, *13*, 757–770. [[CrossRef](#)]

10. Ong, W.J.; Tan, L.L.; Ng, Y.H.; Yong, S.T.; Chai, S.P. Graphitic Carbon Nitride (g-C₃N₄)-Based Photocatalysts for Artificial Photosynthesis and Environmental Remediation: Are We a Step Closer to Achieving Sustainability? *Chem. Rev.* **2016**, *116*, 7159–7329. [[CrossRef](#)]
11. Trickett, C.A.; Helal, A.; Al-Maythaly, B.A.; Yamani, Z.H.; Cordova, K.E.; Yaghi, O.M. The Chemistry of Metal-Organic Frameworks for CO₂ Capture, Regeneration and Conversion. *Nat. Rev. Mater.* **2017**, *2*, 17045. [[CrossRef](#)]
12. Xu, H.Q.; Hu, J.; Wang, D.; Li, Z.; Zhang, Q.; Luo, Y.; Yu, S.H.; Jiang, H.L. Visible-Light Photoreduction of CO₂ in a Metal-Organic Framework: Boosting Electron-Hole Separation via Electron Trap States. *J. Am. Chem. Soc.* **2015**, *137*, 13440–13443. [[CrossRef](#)]
13. Banerjee, T.; Gottschling, K.; Savasci, G.; Ochsenfeld, C.; Lotsch, B.V. H₂ Evolution with Covalent Organic Framework Photocatalysts. *ACS Energy Lett.* **2018**, *3*, 400–409. [[CrossRef](#)]
14. Huang, N.; Wang, P.; Jiang, D. Covalent Organic Frameworks: A Materials Platform for Structural and Functional Designs. *Nat. Rev. Mater.* **2016**, *1*, 16068. [[CrossRef](#)]
15. Chen, Y.; Huang, R.; Chen, D.; Wang, Y.; Liu, W.; Li, X.; Li, Z. Exploring the Different Photocatalytic Performance for Dye Degradations over Hexagonal ZnIn₂S₄ Microspheres and Cubic ZnIn₂S₄ Nanoparticles. *ACS Appl. Mater. Interfaces* **2012**, *4*, 2273–2279. [[CrossRef](#)]
16. Wang, J.; Chen, Y.; Zhou, W.; Tian, G.; Xiao, Y.; Fu, H.; Fu, H. Cubic Quantum Dot/Hexagonal Microsphere ZnIn₂S₄ Heterophase Junctions for Exceptional Visible-Light-Driven Photocatalytic H₂ Evolution. *J. Mater. Chem. A* **2017**, *5*, 8451–8460. [[CrossRef](#)]
17. Tang, M.; Yin, W.; Zhang, F.; Liu, X.; Wang, L. The Potential Strategies of ZnIn₂S₄-Based Photocatalysts for the Enhanced Hydrogen Evolution Reaction. *Front. Chem.* **2022**, *10*, 959414. [[CrossRef](#)]
18. Song, Y.; Zhang, J.; Dong, X.; Li, H. A Review and Recent Developments in Full-Spectrum Photocatalysis Using ZnIn₂S₄-Based Photocatalysts. *Energy Technol.* **2021**, *9*, 2100033. [[CrossRef](#)]
19. Wang, J.; Sun, S.; Zhou, R.; Li, Y.; He, Z.; Ding, H.; Chen, D.; Ao, W. A Review: Synthesis, Modification and Photocatalytic Applications of ZnIn₂S₄. *J. Mater. Sci. Technol.* **2021**, *78*, 1–19. [[CrossRef](#)]
20. Guo, X.; Liu, Y.; Yang, Y.; Mu, Z.; Wang, Y.; Zhang, S.; Wang, S.; Hu, Y.; Liu, Z. Effective Visible-Light Excited Charge Separation in All-Solid-State Ag Bridged BiVO₄/ZnIn₂S₄ Core-Shell Structure Z-Scheme Nanocomposites for Boosting Photocatalytic Organics Degradation. *J. Alloys Compd.* **2021**, *887*, 161389. [[CrossRef](#)]
21. Zhang, T.; Wang, T.; Meng, F.; Yang, M.; Kawi, S. Recent Advances in ZnIn₂S₄-Based Materials towards Photocatalytic Purification, Solar Fuel Production and Organic Transformations. *J. Mater. Chem. C* **2022**, *10*, 5400–5424. [[CrossRef](#)]
22. Shen, J.; Zai, J.; Yuan, Y.; Qian, X. 3D Hierarchical ZnIn₂S₄: The Preparation and Photocatalytic Properties on Water Splitting. *Int. J. Hydrogen Energy* **2012**, *37*, 16986–16993. [[CrossRef](#)]
23. Lin, B.; Li, H.; An, H.; Hao, W.; Wei, J.J.; Dai, Y.; Ma, C.; Yang, G. Preparation of 2D/2D g-C₃N₄ Nanosheet@ZnIn₂S₄ Nanoleaf Heterojunctions with Well-Designed High-Speed Charge Transfer Nanochannels towards High-Efficiency Photocatalytic Hydrogen Evolution. *Appl. Catal. B Environ.* **2018**, *220*, 542–552. [[CrossRef](#)]
24. Yang, G.; Ding, H.; Chen, D.; Feng, J.; Hao, Q.; Zhu, Y. Construction of Urchin-like ZnIn₂S₄-Au-TiO₂ Heterostructure with Enhanced Activity for Photocatalytic Hydrogen Evolution. *Appl. Catal. B Environ.* **2018**, *234*, 260–267. [[CrossRef](#)]
25. Chen, Z.; Guo, F.; Sun, H.; Shi, Y.; Shi, W. Well-Designed Three-Dimensional Hierarchical Hollow Tubular g-C₃N₄/ZnIn₂S₄ Nanosheets Heterostructure for Achieving Efficient Visible-Light Photocatalytic Hydrogen Evolution. *J. Colloid Interface Sci.* **2022**, *607*, 1391–1401. [[CrossRef](#)]
26. Xu, Z.; Shi, W.; Shi, Y.; Sun, H.; Li, L.; Guo, F.; Wen, H. Carbon Dots as Solid-State Electron Mediator and Electron Acceptor in S-Scheme Heterojunction for Boosted Photocatalytic Hydrogen Evolution. *Appl. Surf. Sci.* **2022**, *595*, 153482. [[CrossRef](#)]
27. Cai, Y.; Shi, Y.; Shi, W.; Bai, S.; Yang, S.; Guo, F. A One-Photon Excitation Pathway in 0D/3D CoS₂/ZnIn₂S₄ Composite with Nanoparticles on Micro-Flowers Structure for Boosted Visible-Light-Driven Photocatalytic Hydrogen Evolution. *Compos. Part B Eng.* **2022**, *238*, 109955. [[CrossRef](#)]
28. Wang, J.; Shi, Y.; Sun, H.; Shi, W.; Guo, F. Fabrication of Bi₄Ti₃O₁₂/ZnIn₂S₄ S-Scheme Heterojunction for Achieving Efficient Photocatalytic Hydrogen Production. *J. Alloy. Compd.* **2023**, *930*, 167450. [[CrossRef](#)]
29. Shi, Y.; Li, L.; Xu, Z.; Qin, X.; Cai, Y.; Zhang, W.; Shi, W.; Du, X.; Guo, F. Coupled Internal Electric Field with Hydrogen Release Kinetics for Promoted Photocatalytic Hydrogen Production through Employing Carbon Coated Transition Metal as Co-Catalyst. *J. Colloid Interface Sci.* **2023**, *630*, 274–285. [[CrossRef](#)]
30. Chen, K.; Shi, Y.; Shu, P.; Luo, Z.; Shi, W.; Guo, F. Construction of Core-Shell FeS₂@ZnIn₂S₄ Hollow Hierarchical Structure S-Scheme Heterojunction for Boosted Photothermal-Assisted Photocatalytic H₂ Production. *Chem. Eng. J.* **2023**, *454*, 140053. [[CrossRef](#)]
31. Shi, Y.; Li, L.; Xu, Z.; Guo, F.; Shi, W. Construction of Full Solar-Spectrum Available S-Scheme Heterojunction for Boosted Photothermal-Assisted Photocatalytic H₂ Production. *Chem. Eng. J.* **2023**, *459*, 141549. [[CrossRef](#)]
32. Yang, G.; Chen, D.; Ding, H.; Feng, J.; Zhang, J.Z.; Zhu, Y.; Hamid, S.; Bahnemann, D.W. Well-Designed 3D ZnIn₂S₄ Nanosheets/TiO₂ Nanobelts as Direct Z-Scheme Photocatalysts for CO₂ Photoreduction into Renewable Hydrocarbon Fuel with High Efficiency. *Appl. Catal. B Environ.* **2017**, *219*, 611–618. [[CrossRef](#)]
33. Xia, Y.; Cheng, B.; Fan, J.; Yu, J.; Liu, G. Near-Infrared Absorbing 2D/3D ZnIn₂S₄/N-Doped Graphene Photocatalyst for Highly Efficient CO₂ Capture and Photocatalytic Reduction. *Sci. China Mater.* **2020**, *63*, 552–565. [[CrossRef](#)]
34. Cheng, C.; Chen, D.; Li, N.; Xu, Q.; Li, H.; He, J.; Lu, J. ZnIn₂S₄ Grown on Nitrogen-Doped Hollow Carbon Spheres: An Advanced Catalyst for Cr(VI) Reduction. *J. Hazard. Mater.* **2020**, *391*, 122205. [[CrossRef](#)]

35. Mu, F.; Cai, Q.; Hu, H.; Wang, J.; Wang, Y.; Zhou, S.; Kong, Y. Construction of 3D Hierarchical Microarchitectures of Z-Scheme UiO-66-(COOH)₂/ZnIn₂S₄ Hybrid Decorated with Non-Noble MoS₂ Cocatalyst: A Highly Efficient Photocatalyst for Hydrogen Evolution and Cr(VI) Reduction. *Chem. Eng. J.* **2020**, *384*, 123352. [[CrossRef](#)]
36. Qiu, J.; Li, M.; Yang, L.; Yao, J. Facile Construction of Three-Dimensional Netted ZnIn₂S₄ by Cellulose Nanofibrils for Efficiently Photocatalytic Reduction of Cr(VI). *Chem. Eng. J.* **2019**, *375*, 121990. [[CrossRef](#)]
37. Zhang, J.; Pan, Z.H.; Yang, Y.; Wang, P.F.; Pei, C.Y.; Chen, W.; Huang, G.B. Boosting the Catalytic Activity of a Step-Scheme In₂O₃/ZnIn₂S₄ Hybrid System for the Photofixation of Nitrogen. *Chin. J. Catal.* **2022**, *43*, 265–275. [[CrossRef](#)]
38. Chen, S.; Xie, F.; Wang, X.; Zhao, X.; Tang, Z. Efficient Charge Separation between ZnIn₂S₄ Nanoparticles and Polyaniline Nanorods for Nitrogen Photofixation. *New J. Chem.* **2020**, *44*, 7350–7356. [[CrossRef](#)]
39. Guo, L.; Han, X.; Zhang, K.; Zhang, Y.; Zhao, Q.; Wang, D.; Feng, F. Heterostructure with Enhanced Photocatalytic Activity for N₂ Fixation and Phenol Degradation. *Catal.* **2019**, *9*, 729. [[CrossRef](#)]
40. Shi, W.; Lv, H.; Yuan, S.; Huang, H.; Liu, Y.; Kang, Z. Synergetic Effect of Carbon Dots as Co-Catalyst for Enhanced Photocatalytic Performance of Methyl Orange on ZnIn₂S₄ Microspheres. *Sep. Purif. Technol.* **2017**, *174*, 282–289. [[CrossRef](#)]
41. Hao, C.C.; Tang, Y.B.; Shi, W.L.; Chen, F.Y.; Guo, F. Facile Solvothermal Synthesis of a Z-Scheme 0D/3D CeO₂/ZnIn₂S₄ Heterojunction with Enhanced Photocatalytic Performance under Visible Light Irradiation. *Chem. Eng. J.* **2021**, *409*, 128168. [[CrossRef](#)]
42. Shi, W.; Hao, C.; Fu, Y.; Guo, F.; Tang, Y.; Yan, X. Enhancement of Synergistic Effect Photocatalytic/Persulfate Activation for Degradation of Antibiotics by the Combination of Photo-Induced Electrons and Carbon Dots. *Chem. Eng. J.* **2022**, *433*, 133741. [[CrossRef](#)]
43. Shi, W.; Hao, C.; Shi, Y.; Guo, F.; Tang, Y. Effect of Different Carbon Dots Positions on the Transfer of Photo-Induced Charges in Type I Heterojunction for Significantly Enhanced Photocatalytic Activity. *Sep. Purif. Technol.* **2023**, *304*, 122337. [[CrossRef](#)]
44. Yang, Y.; Tan, H.; Cheng, B.; Fan, J.; Yu, J.; Ho, W. Near-Infrared-Responsive Photocatalysts. *Small Methods* **2021**, *5*, 2001042. [[CrossRef](#)]
45. Sudhaik, A.; Parwaz Khan, A.A.; Raizada, P.; Nguyen, V.H.; Van Le, Q.; Asiri, A.M.; Singh, P. Strategies Based Review on Near-Infrared Light-Driven Bismuth Nanocomposites for Environmental Pollutants Degradation. *Chemosphere* **2022**, *291*, 132781. [[CrossRef](#)]
46. Tian, Q.; Yao, W.; Wu, W.; Jiang, C. NIR Light-Activated Upconversion Semiconductor Photocatalysts. *Nanoscale Horiz.* **2019**, *4*, 10–25. [[CrossRef](#)]
47. Liu, T.; Liu, B.; Yang, L.; Ma, X.; Li, H.; Yin, S.; Sato, T.; Sekino, T.; Wang, Y. RGO/Ag₂S/TiO₂ Ternary Heterojunctions with Highly Enhanced UV-NIR Photocatalytic Activity and Stability. *Appl. Catal. B Environ.* **2017**, *204*, 593–601. [[CrossRef](#)]
48. Gannoruwa, A.; Niroshan, K.; Ileperuma, O.A.; Bandara, J. Infrared Radiation Active, Novel Nanocomposite Photocatalyst for Water Splitting. *Int. J. Hydrog. Energy* **2014**, *39*, 15411–15415. [[CrossRef](#)]
49. Tian, J.; Sang, Y.; Yu, G.; Jiang, H.; Mu, X.; Liu, H. A Bi₂WO₆-Based Hybrid Photocatalyst with Broad Spectrum Photocatalytic Properties under UV, Visible, and near-Infrared Irradiation. *Adv. Mater.* **2013**, *25*, 5075–5080. [[CrossRef](#)]
50. Du, C.; Yan, B.; Yang, G. Promoting Photocatalytic Hydrogen Evolution by Introducing Hot Islands: SnSe Nanoparticles on ZnIn₂S₄ Monolayer. *Chem. Eng. J.* **2021**, *404*, 126477. [[CrossRef](#)]
51. Sang, Y.; Liu, H.; Umar, A. Photocatalysis from UV/Vis to near-Infrared Light: Towards Full Solar-Light Spectrum Activity. *ChemCatChem* **2015**, *7*, 559–573. [[CrossRef](#)]
52. Wang, L.; Xu, X.; Cheng, Q.; Dou, S.X.; Du, Y. Near-Infrared-Driven Photocatalysts: Design, Construction, and Applications. *Small* **2021**, *17*, 1904107. [[CrossRef](#)]
53. Guo, X.; Peng, Y.; Liu, G.; Xie, G.; Guo, Y.; Zhang, Y.; Yu, J. An Efficient ZnIn₂S₄@CuInS₂ Core-Shell P-n Heterojunction to Boost Visible-Light Photocatalytic Hydrogen Evolution. *J. Phys. Chem. C* **2020**, *124*, 5934–5943. [[CrossRef](#)]
54. Liu, J.; Jataw, S.; Herber, M.; Hill, E.H. Few-Layer ZnIn₂S₄/Laponite Heterostructures: Role of Mg²⁺ Leaching in Zn Defect Formation. *Langmuir* **2021**, *37*, 4727–4735. [[CrossRef](#)]
55. Chen, Z.; Shi, Y.; Lu, J.; Cao, L.; Tian, Y.; Chen, L.; Guo, F.; Shi, W. Three-Dimensional NaYF₄:Yb³⁺/Tm³⁺ Hexagonal Prisms Coupled with ZnIn₂S₄ nanosheets for Boosting near-Infrared Photocatalytic H₂ evolution. *J. Environ. Chem. Eng.* **2022**, *10*, 108352. [[CrossRef](#)]
56. Luo, D.; Peng, L.; Wang, Y.; Lu, X.; Yang, C.; Xu, X.; Huang, Y.; Ni, Y. Highly Efficient Photocatalytic Water Splitting Utilizing a WO_{3-x}/ZnIn₂S₄ ultrathin Nanosheet Z-Scheme Catalyst. *J. Mater. Chem. A* **2021**, *9*, 908–914. [[CrossRef](#)]
57. Song, J.; Jiang, T.; Ji, G.; Zhang, W.; Cheng, X.; Weng, W.; Zhu, L.; Xu, X. Visible-Light-Driven Dye Degradation Using a Floriated ZnIn₂S₄/AgIn₅S₈ Heteromicrosphere Catalyst. *RSC Adv.* **2015**, *5*, 95943–95952. [[CrossRef](#)]
58. Yu, M.; Lv, X.; Mahmoud Idris, A.; Li, S.; Lin, J.; Lin, H.; Wang, J.; Li, Z. Upconversion Nanoparticles Coupled with Hierarchical ZnIn₂S₄ Nanorods as a Near-Infrared Responsive Photocatalyst for Photocatalytic CO₂ Reduction. *J. Colloid Interface Sci.* **2022**, *612*, 782–791. [[CrossRef](#)]
59. Xu, H.; Jiang, Y.; Yang, X.; Li, F.; Li, A.; Liu, Y.; Zhang, J.; Zhou, Z.; Ni, L. Fabricating Carbon Quantum Dots Doped ZnIn₂S₄ Nanoflower Composites with Broad Spectrum and Enhanced Photocatalytic Tetracycline Hydrochloride Degradation. *Mater. Res. Bull.* **2018**, *97*, 158–168. [[CrossRef](#)]
60. Jiang, R.; Wu, D.; Lu, G.; Yan, Z.; Liu, J. Modified 2D-2D ZnIn₂S₄/BiOCl van Der Waals Heterojunctions with CQDs: Accelerated Charge Transfer and Enhanced Photocatalytic Activity under Vis- and NIR-Light. *Chemosphere* **2019**, *227*, 82–92. [[CrossRef](#)]

61. Wu, C.; Xing, Z.; Fang, B.; Cui, Y.; Li, Z.; Zhou, W. Polyoxometalate-Based Yolk@shell Dual Z-Scheme Superstructure Tandem Heterojunction Nanoreactors: Encapsulation and Confinement Effects. *J. Mater. Chem. A* **2022**, *10*, 180–191. [[CrossRef](#)]
62. Lu, Y.; Jia, X.; Ma, Z.; Li, Y.; Yue, S.; Liu, X.; Zhang, J. W^{5+} - W^{5+} Pair Induced LSPR of $W_{18}O_{49}$ to Sensitize $ZnIn_2S_4$ for Full-Spectrum Solar-Light-Driven Photocatalytic Hydrogen Evolution. *Adv. Funct. Mater.* **2022**, *32*, 2203638. [[CrossRef](#)]
63. An, H.; Lv, Z.; Zhang, K.; Deng, C.; Wang, H.; Xu, Z.; Wang, M.; Yin, Z. Plasmonic Coupling Enhancement of Core-Shell Au@Pt Assemblies on $ZnIn_2S_4$ Nanosheets towards Photocatalytic H_2 Production. *Appl. Surf. Sci.* **2021**, *536*, 147934. [[CrossRef](#)]
64. Cao, S.; Yan, X.; Kang, Z.; Liang, Q.; Liao, X.; Zhang, Y. Band Alignment Engineering for Improved Performance and Stability of $ZnFe_2O_4$ Modified CdS/ZnO Nanostructured Photoanode for PEC Water Splitting. *Nano Energy* **2016**, *24*, 25–31. [[CrossRef](#)]
65. Bai, Z.; Yan, X.; Li, Y.; Kang, Z.; Cao, S.; Zhang, Y. 3D-Branched ZnO/CdS Nanowire Arrays for Solar Water Splitting and the Service Safety Research. *Adv. Energy Mater.* **2016**, *6*, 1501459. [[CrossRef](#)]
66. Jiang, L.; Zhou, S.; Yang, J.; Wang, H.; Yu, H.; Chen, H.; Zhao, Y.; Yuan, X.; Chu, W.; Li, H. Near-Infrared Light Responsive TiO_2 for Efficient Solar Energy Utilization. *Adv. Funct. Mater.* **2022**, *32*, 2108977. [[CrossRef](#)]
67. Liu, R.; Li, H.; Duan, L.; Shen, H.; Zhang, Y.; Zhao, X. In Situ Synthesis and Enhanced Visible Light Photocatalytic Activity of C- TiO_2 Microspheres/Carbon Quantum Dots. *Ceram. Int.* **2017**, *43*, 8648–8654. [[CrossRef](#)]
68. Zhang, X.; Ming, H.; Liu, R.; Han, X.; Kang, Z.; Liu, Y.; Zhang, Y. Highly Sensitive Humidity Sensing Properties of Carbon Quantum Dots Films. *Mater. Res. Bull.* **2013**, *48*, 790–794. [[CrossRef](#)]
69. Rama Krishna, C.; Im, Y.; Kang, M. Nitrogen Doped Carbon Quantum Dots as a Green Luminescent Sensitizer to Functionalize ZnO Nanoparticles for Enhanced Photovoltaic Conversion Devices. *Mater. Res. Bull.* **2017**, *94*, 399–407. [[CrossRef](#)]
70. Hong, Y.; Meng, Y.; Zhang, G.; Yin, B.; Zhao, Y.; Shi, W.; Li, C. Facile Fabrication of Stable Metal-Free CQDs/g- C_3N_4 Heterojunctions with Efficiently Enhanced Visible-Light Photocatalytic Activity. *Sep. Purif. Technol.* **2016**, *171*, 229–237. [[CrossRef](#)]
71. Zhang, P.; Wang, T.; Gong, J. Mechanistic Understanding of the Plasmonic Enhancement for Solar Water Splitting. *Adv. Mater.* **2015**, *27*, 5328–5342. [[CrossRef](#)]
72. Lincic, S.; Christopher, P.; Ingram, D.B. Plasmonic-Metal Nanostructures for Efficient Conversion of Solar to Chemical Energy. *Nat. Mater.* **2011**, *10*, 911–921. [[CrossRef](#)]
73. Valenti, M.; Jonsson, M.P.; Biskos, G.; Schmidt-Ott, A.; Smith, W.A. Plasmonic Nanoparticle-Semiconductor Composites for Efficient Solar Water Splitting. *J. Mater. Chem. A* **2016**, *4*, 17891–17912. [[CrossRef](#)]
74. Xu, J.; Yang, W.M.; Huang, S.J.; Yin, H.; Zhang, H.; Radjenovic, P.; Yang, Z.L.; Tian, Z.Q.; Li, J.F. CdS Core-Au Plasmonic Satellites Nanostructure Enhanced Photocatalytic Hydrogen Evolution Reaction. *Nano Energy* **2018**, *49*, 363–371. [[CrossRef](#)]
75. Sun, S.; Liu, H.; Wu, L.; Png, C.E.; Bai, P. Interference-Induced Broadband Absorption Enhancement for Plasmonic-Metal@semiconductor Microsphere as Visible Light Photocatalyst. *ACS Catal.* **2014**, *4*, 4269–4276. [[CrossRef](#)]
76. Yu, G.; Qian, J.; Zhang, P.; Zhang, B.; Zhang, W.; Yan, W.; Liu, G. Collective Excitation of Plasmon-Coupled Au-Nanochain Boosts Photocatalytic Hydrogen Evolution of Semiconductor. *Nat. Commun.* **2019**, *10*, 1–8. [[CrossRef](#)]
77. Coughlan, C.; Ibáñez, M.; Dobrozhan, O.; Singh, A.; Cabot, A.; Ryan, K.M. Compound Copper Chalcogenide Nanocrystals. *Chem. Rev.* **2017**, *117*, 5865–6109. [[CrossRef](#)]
78. Zhang, Z.; Huang, J.; Fang, Y.; Zhang, M.; Liu, K.; Dong, B. A Nonmetal Plasmonic Z-Scheme Photocatalyst with UV- to NIR-Driven Photocatalytic Protons Reduction. *Adv. Mater.* **2017**, *29*, 1606688. [[CrossRef](#)]
79. Ji, M.; Xu, M.; Zhang, W.; Yang, Z.; Huang, L.; Liu, J.; Zhang, Y.; Gu, L.; Yu, Y.; Hao, W.; et al. Structurally Well-Defined Au@ Cu_2 -XS Core-Shell Nanocrystals for Improved Cancer Treatment Based on Enhanced Photothermal Efficiency. *Adv. Mater.* **2016**, *28*, 3094–3101. [[CrossRef](#)]
80. Kasani, S.; Zheng, P.; Bright, J.; Wu, N. Tunable Visible-Light Surface Plasmon Resonance of Molybdenum Oxide Thin Films Fabricated by E-beam Evaporation. *ACS Appl. Electron. Mater.* **2019**, *1*, 2389–2395. [[CrossRef](#)]
81. Zhang, Z.; Jiang, X.; Liu, B.; Guo, L.; Lu, N.; Wang, L.; Huang, J.; Liu, K.; Dong, B. IR-Driven Ultrafast Transfer of Plasmonic Hot Electrons in Nonmetallic Branched Heterostructures for Enhanced H_2 Generation. *Adv. Mater.* **2018**, *30*, 1705221. [[CrossRef](#)] [[PubMed](#)]

Disclaimer/Publisher's Note: The statements, opinions and data contained in all publications are solely those of the individual author(s) and contributor(s) and not of MDPI and/or the editor(s). MDPI and/or the editor(s) disclaim responsibility for any injury to people or property resulting from any ideas, methods, instructions or products referred to in the content.